International Journal of Thermal Sciences 48 (2009) 1338–1347

Contents lists available at ScienceDirect

International Journal of Thermal Sciences

www.elsevier.com/locate/ijts

Accelerating ray convergence in incident heat flux calculations using Sobol sequences

P.S. Cumber *

Heriot-Watt University, School of Engineering and Physical Sciences, Riccarton Campus, Edinburgh, United Kingdom

ARTICLE INFO

Article history:
Received 24 December 2007
Received in revised form 13 August 2008
Accepted 4 November 2008
Available online 5 December 2008

Keywords:
Thermal radiation modelling
Ray effect
Monte-Carlo method
Jet fires
Sobol sequences

ABSTRACT

In this paper an improved quadrature scheme based on the reverse Monte Carlo method implemented using Sobol sequences to generate ray orientations is presented. This has the property that a more uniform pattern of rays on the unit hemisphere is produced compared to the usual implementation of the reverse Monte Carlo method. The use of Sobol sequences gives a ray convergence rate for the incident heat flux that is asymptotically equivalent to $O(N_{\mathrm{Ray}}^{-1})$. The generation of ray directions using Sobol sequences means that the Central Limit Theorem no longer holds. In its place a Gaussian variable is formulated from the incident intensity distributions calculated using Sobol sequences. This makes it possible to calculate confidence limits for a prediction of incident heat flux and the confidence limits contract with ray number at a rate of $O(N_{\mathrm{Ray}}^{-1}ln(N_{\mathrm{Ray}}))$. An extension to the Monte Carlo method combined with Sobol sequences is also presented that exploits the shape of the incident intensity distribution to a receiver. The new methodology is relatively simple to implement and shows some promising improvements in computational efficiency.

1. Introduction

A jet fire is highly directional with source momentum dominating the fire dynamics in the near field compared to further downstream where the buoyancy of the fire becomes influential [1]. The simulation of jet fires is of interest when assessing the safety of high pressure plant processing hydrocarbons [2]. A pipe fracture or leak due to corrosion or third party interference will often result in a jet of gas. The jet of gas may spontaneously ignite or disperse and on finding a source of ignition light back to the source, in either case a jet fire will form. As well as being important in industrial safety jet fires are also of interest as a generic flow used for investigating high speed reacting shear flows. Experimentally jet fires are relatively simple to produce in the laboratory with many experimental studies presented in the open literature with different fuels, some of the fires are rim-stabilised [3,4] and some are lifted [5]. In these papers detailed measurements characterising the flame structure, such as the mean temperature, velocity fields, turbulence parameters and chemical species are presented. In addition measurements of the received heat flux field external to the fire and spectral intensity distribution for pencils of radiation through the fire can be found in the open literature. The experimental data taken in these studies has proved invaluable for the development and validation of mathematical models of jet fires [6–8].

The focus of this paper is the efficient calculation of incident heat flux distributions surrounding a jet fire. In jet fires the radiation field is highly anisotropic in nature with a relatively small hot volume of gas dominating the field of view of the receivers external to the fire. The anisotropy means that the direction cosine dependence of the intensity field must be modelled using an approach that allows the accurate evaluation of the heat flux integral. One approach that is numerically exact for anisotropic radiation fields is one that includes ray tracing as a component of the solution strategy such as that used in the discrete transfer method [9,10] and the reverse Monte Carlo method [11,12]. Ray tracing can be a potentially time consuming process, the computational time being sensitive to the number of rays used and the fineness of representation of the flame structure on a finite volume mesh. A further complication depending on the fuel and the scale of the jet fire is the spectral intensity distribution of a pencil of radiation is banded in nature. This makes the grey gas approximation invalid adding to the computational cost as a numerical integration of the spectral intensity distribution is required to evaluate the incident intensity. If the jet fire is turbulent which is the case in the industrial safety context thermal emission again depending on the fuel type and scale is sensitive to the fluctuations in the temperature and participating species fields. This is turbulence-radiation interaction [13]. The nonlinear dependence of the Plank distribution on temperature means that there is a tendency for more radiation to

* Tel.: +44 (0)131 451 3532; fax: +44 (0)131 451 3129.
E-mail address: p.s.cumber@hw.ac.uk.

1290-0729/$ – see front matter
doi:10.1016/j.ijthermalsci.2008.11.007

Nomenclature

A, A_1	constants in convergence rate expressions
d	nozzle diameter (m), dimension of a hypercube
I^-	spectrally integrated incident intensity ($W m^{-2} str^{-1}$)
I_{bg}	background intensity
$\underline{n}$	receiver orientation
N_{Ray}	number of rays
N_{Trace}	number of rays traced
N_φ, N_θ	number of rays in the φ and θ directions
P	probability density function
q_{inc}	radiation heat flux ..... ($W m^{-2}$)
r	radial co-ordinate ..... (m)
R_{min}	distance to the hot ray set for a given ray
R_φ, R_θ	pseudo random numbers
$S_{cold\ ray}$	cold ray set
$S_{hot\ ray}$	hot ray set
V_i	direction numbers
$\underline{x}$	point vector
X_i, Y_i	transformed coordinates for a rays orientation
z	axial co-ordinate ..... (m)

Greek symbols

$\Delta\varphi, \Delta\theta$	ray spacing in the φ and θ directions
φ, θ	spherical co-ordinates
Ω	solid angle ..... (str)
σ	Stefan Boltzmann constant ..... ($W m^{-2} K^{-4}$)
$\sigma_{I\cos\sin}$	sample variance

Subscripts

amb	ambient value

be emitted from a turbulent fire than an analysis based on the mean flow fields would suggest.

For laboratory scale natural gas jet fires, turbulence-radiation interaction can be neglected as there is a body of work that shows these effects are negligible [4,14]. In this paper the efficient quadrature of the incident heat flux is considered such that the anisotropy of the radiation field is accounted for.

2. Evaluation of the heat flux

When calculating the thermal radiation field for any combusting system an important property is the incident heat flux to a given point and surface orientation

$$q_{inc}(\underline{x}, \underline{n}) = \int_0^{2\pi} \int_0^{\pi/2} I^-(\varphi, \theta) \cos\theta \sin\theta \, d\theta \, d\varphi \tag{1}$$

where φ and θ are spherical co-ordinates on the unit hemisphere. $\underline{x}$ is a position vector, and $\underline{n}$ is an orientation vector. $I^-(\varphi, \theta)$ represents the spectrally integrated incident intensity distribution, $\cos\theta$ is introduced to account for Lambert's cosine law [15] and the remaining terms represent a differential area on the unit hemisphere.

For jet fires the numerical evaluation of the incident flux integral, (1) is non-trivial as the anisotropy of the radiation field means that the incident intensity is significantly above the background radiation levels on a small portion of the field of view. As a consequence, to get a reasonable estimate of the incident flux the incident intensity distribution must be evaluated using many rays.

The ray effect is a property of the source of radiation and the ray distribution used in the quadrature scheme [16]. If a source of radiation emits in a direction not in the set of directions given by the set of rays the predicted incident heat flux will be in error [17,18]. The significance of the ray effect is diminished if a finer ray mesh is used, but at increased computational cost. The ray effect has been investigated for the most part in the context of the discrete ordinates method [17–19], although it is present in any deterministic radiation solver. When the radiation field is anisotropic poor numerical behaviour such as slow convergence with respect to the number of rays used, oscillatory convergence and in some cases physically unrealistic predictions of the radiation field can occur. Oscillatory convergence is a problem as any error estimation technique based on extrapolation will fail under these conditions. For the standard quadrature scheme implemented in the discrete transfer method [9] the theoretical ray convergence rate is $O(N_{Ray}^{-1})$. The convergence rate is derived using a regularity assumption on the incident intensity distribution. However for jet fires the regularity assumption is only valid when the ray distribution is sufficiently fine. This is one of the reasons for the ray effect in jet fires. Another reason for the ray effect is the shape of the fire, a long and thin flame means the predicted incident heat flux exhibits sensitivity to the ray mesh prescribed in the angle of rotation.

The first calculations of the incident heat flux surrounding a jet fire using the discrete transfer method were presented by Jeng and Faeth [20]. Jeng and Faeth proposed a methodology for calculating the incident heat flux and compared the predicted heat flux with the measured heat flux for two lines of receivers and three laboratory scale natural gas jet fires. Space limitations prevented them from demonstrating a detailed ray convergence analysis but they estimated that the numerical error was of the order of 10% using 84 rays per receiver. Subsequently Cumber [21] presented a detailed ray convergence study for Jeng and Faeth's jet fires indicating the poor convergence property of ray tracing techniques applied to the external radiation field of jet fires.

2.1. Ray effect mitigation strategies in jet fires

The ray effect is well known in the thermal radiation modelling community [16] and a number of papers in the open literature have focussed on quantifying the ray effect [16] and investigating a range of numerical techniques to improve performance [21–24].

A stochastic technique that has been previously advocated for mitigating the ray effect in fires is the reverse Monte Carlo method [12]. In this technique the ray directions are generated using a pseudo random number generator [25] based on a given probability density function. This allows the mean of a given function of the intensity distribution to be evaluated. A number of alternative implementations of the Monte Carlo method applied to (1) were considered in the development of the methodology presented below and the following was found to deliver the best convergence behaviour when applied to jet fires. The incident flux integral (1) is approximated as,

$$q_{inc} = \pi^2 \overline{I^- \cos\theta \sin\theta} \tag{2}$$

and

$$\overline{I^- \cos\theta \sin\theta} = \frac{1}{N_{Ray}} \sum_{i=1}^{N_{Ray}} I^-(\varphi_i, \theta_i) \times \cos\theta_i \sin\theta_i$$

The ray directions are given by simulating pseudo random numbers that have an appropriate probability distribution.

$$R_\theta = \frac{\int_0^\theta d\theta}{\int_0^{\pi/2} d\theta} = \frac{2\theta_i}{\pi} \qquad (3)$$

$$R_\varphi = \frac{\int_0^\varphi d\varphi}{\int_0^{2\pi} d\varphi} = \frac{\varphi_i}{2\pi}$$

where R_θ and R_φ are pseudo random numbers in the unit interval. This is a stochastic method that has some advantages over deterministic approaches. As the ray directions are chosen pseudo randomly the possibility of physically incorrect maxima and minima in the incident heat flux distribution can in theory be reduced. This is because a continuous intensity distribution is not being replaced by a discrete set of rays arranged to form a mesh on the unit hemisphere. The second advantage of the Monte Carlo method is a consequence of the Central Limit Theorem [26], as confidence limits for the predicted incident heat flux can be calculated. This is a useful tool but it also exhibits one of the major weaknesses of the Monte Carlo method as the Central Limit Theorem can also be interpreted as a convergence result with a convergence rate of $O(N_{\mathrm{Ray}}^{-0.5})$. This is a poor result in comparison to most deterministic quadrature schemes. Choi et al. [12] report for their heptane pool fire simulations using the reverse Monte Carlo method, 10,000 rays were required to produce ray independent predictions of the radiative heat flux to the pool surface. It should be noted that they also completed some simulations using 100,000 rays to confirm the ray independence.

Another weakness that is sometimes cited for Monte Carlo methods is the pseudo random numbers are a significant overhead compared to ray direction specification for deterministic quadrature schemes. This is not the case in this application as the ray tracing algorithm required to determine the temperature and participating species profiles along a ray is a significant cost. The spectral integration using in this case a narrow band radiation model, RADCAL [27–29] is also a significant computational cost making the ray direction generation trivial in comparison.

All of the ray effect mitigation strategies discussed above and in [21–24] have weaknesses to do with difficulty of implementation and effectiveness at accelerating ray convergence. In this article a quadrature strategy is presented that goes someway to improving the situation. Before the quadrature scheme is presented the mathematical model used to calculate the flame structure is considered.

3. Jet fire model

The basis of the flow equations is the parabolised Favre averaged Navier Stokes equations in an axisymmetric coordinate system [30]. The system is closed using a variant of the k–ε turbulence model [31,32]. The version of the k–ε turbulence model is a modification of the standard implementation of the k–ε turbulence model [32] to take account of the round jet/plane jet anomaly [33,34].

The jet fire model accounts for turbulent combustion using a laminar flamelet combustion model [35]. Combustion is assumed to be infinitely fast with a prescribed probability density function, a β function. The shape of the β function at any spatial location is determined by a conserved scalar, the mixture fraction and its variance, which are calculated using modelled transport equations [35]. To account for radiation heat loss a transport equation for a specific enthalpy perturbation is solved, where radiation heat loss is introduced using the optically thin approximation [16]. This approach is more sophisticated than accounting for the radiative heat loss by adjusting the temperature flamelet and has been used successfully in other computational studies [6,31,36]. The incident heat flux calculations and the flame structure model are uncoupled. This makes it possible to implement the methodology on relatively modest computer facilities and still calculate the flow and radiation properties accurately [2,4,6–8,35].

In the jet fire simulation presented below the bulk inlet conditions are given by the nozzle diameter and the average source velocity. The mean stream-wise velocity distribution and radial velocity distribution are taken to be consistent with fully developed pipe flow. Nozzle exit turbulence profiles are calculated by assuming the turbulence is isotropic and in equilibrium. A uniform turbulence velocity of 5% of the source velocity is specified.

For all simulations in this article 40 control volumes in the radial co-ordinate direction spanning the jet radius are used to calculate the flame structure. In the axial direction a maximum fractional step of less than 2% of the radial control volume spacing is used. A number of simulations using 80 control volumes were also completed to confirm that the predictions presented are independent of further mesh refinement. Using a Dual Intel(R) Core TM 2 processor with a clock speed of 1.8 GHz the flame structure model took approximately 27 seconds to complete a simulation with 40 control volumes in the radial direction.

As mentioned above spectral emission from the fire is modelled using a statistical narrow band model, RADCAL [27,28]. To mirror the spectral characteristics of the radiometers used in the experiment the predictions of the spectrally integrated intensity were evaluated from integrations over the spectral window, 1–6.5 μm. In the spectral integrations approximately 300–400 narrow bands were used. The radiometers used to measure the incident heat flux had a field of view of 150° cone angle; this was taken into account in the simulations presented below.

4. Jet fire simulation

The mathematical model for the flame structure described above has been validated previously, producing accurate representations of the mean temperature field and participating species [6,29]. As the interest is the incident heat flux distribution, one natural gas jet fire experiment is considered where detailed heat flux and mean temperature measurements are available [3]. The source of the jet fire is a 5 mm diameter nozzle with an average gas velocity of 49 m/sec [3,4].

4.1. Fire structure

This paper is concerned with the efficient quadrature of the incident heat flux integral (1), but before this can be considered it is important to confirm that the underlying model provides a reasonably accurate representation of reality. By way of illustration the predicted and measured radial mean temperature distribution at a number of axial locations is shown in Fig. 1. As can be seen from the figure the level of agreement is satisfactory and typical for this type of jet fire model.

4.2. Incident heat flux distribution

Having established the flame structure is well represented by the flow model, Fig. 2a and b shows the measured and predicted incident heat flux for two lines of receivers. In these figures the predicted incident heat flux distributions are calculated using the quadrature formula implemented as part of the discrete transfer method, with ray distributions that are uniformly spaced in the angle of incidence, θ and angle of rotation, φ. Fig. 2a shows the incident heat flux distribution for a horizontal line of receivers. These receivers have a vertical orientation and are located in the plane of the nozzle exit ($z = 0$). Fig. 2b shows the heat flux distribution for a vertical line of receivers with a horizontal orientation directed towards the flame axis. The line of receivers is located at a radial distance of $r = 0.575$ m from the flame axis. For the predicted heat flux distributions 3072 rays per receiver were used. As will be demonstrated below the predicted heat flux distributions

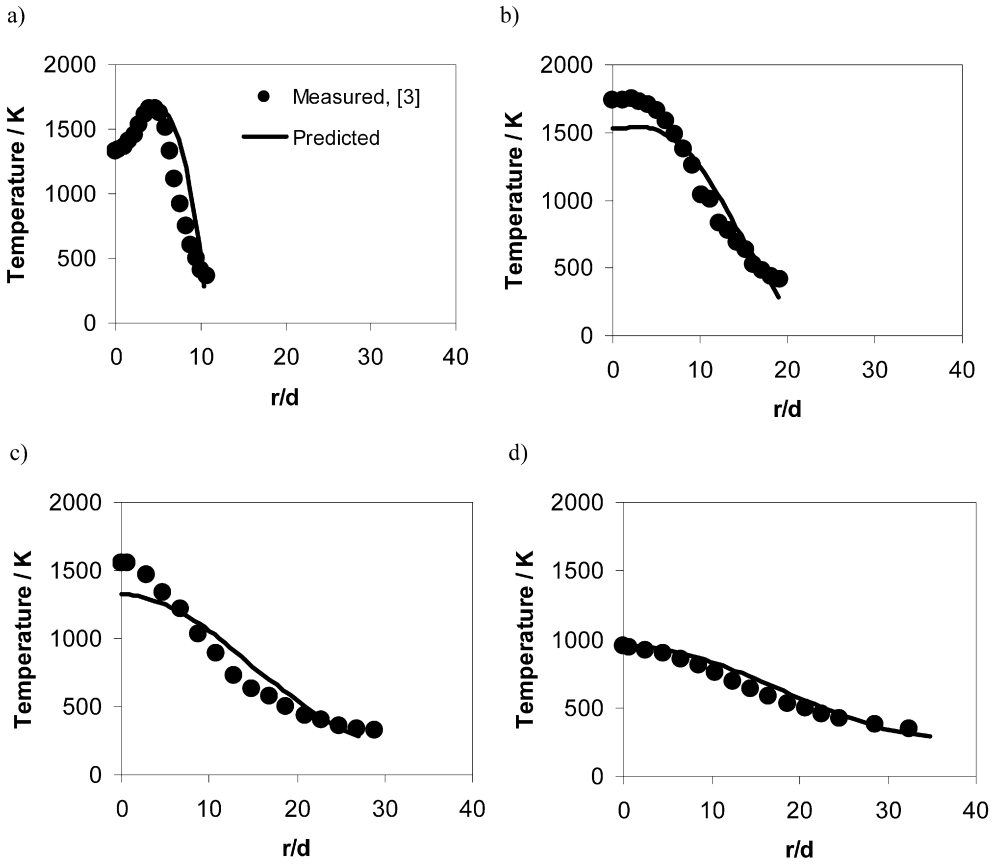

Fig. 1. Predicted and measured radial mean temperature distributions at four axial locations, (a) $z/d = 52.5$, (b) $z/d = 102$, (c) $z/d = 150$, and (d) $z/d = 198$.

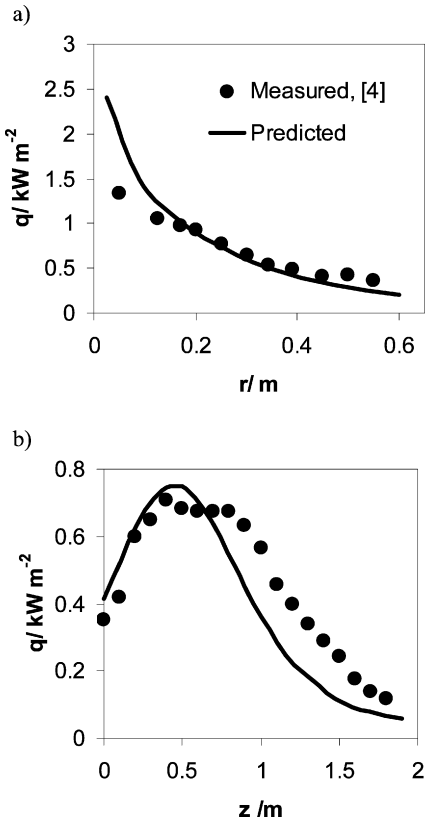

Fig. 2. Measured and predicted incident heat flux to (a) an horizontal line of receivers at $z = 0$ m and (b) a vertical line of receivers located at $r = 0.575$ m.

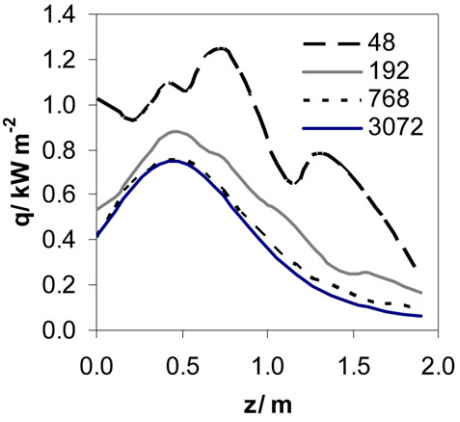

Fig. 3. A ray refinement study of the incident heat flux to a vertical line of receivers, $r = 0.575$ m using a deterministic quadrature scheme.

shown in Fig. 2a and b are insensitive to further ray refinement. The agreement between the measured and predicted distributions is reasonably close. The tendency to underpredict the heat flux distribution in the far field could be due to the neglect of turbulence-radiation effects although a previous study [4] has shown that such effects for laboratory scale natural gas jets are small.

5. Demonstration of the ray effect

As mentioned above the predicted heat flux distributions shown in Fig. 2a and b were calculated with 3072 rays per receiver. This was determined to be sufficiently accurate as further ray mesh refinement does not change the predicted distribution to the resolution of the figure. Fig. 3 shows the predicted incident heat flux

distribution for the vertical line of receivers calculated using four different ray distributions. A course ray mesh of 48 rays and three further ray distributions calculated by successively quadrupling the number of rays as the hemisphere is a two-dimensional manifold. The 48 ray and 192 ray predicted heat flux distributions are physically incorrect with multiple local maxima present. This is typical behaviour where the heat flux distribution is dominated by a small hot volume of emitting gas, i.e. the ray effect is significant. The 3072 ray prediction of the incident heat flux distribution was confirmed to be insensitive to further ray refinement by comparing it to a predicted heat flux distribution calculated with 12,288 rays. In the simulations presented in Figs. 2 and 3 the ray meshes in the θ and φ directions are maintained at a 1:3 ratio.

The influence of the ray effect on the ray convergence behaviour in jet fires has been considered previously. Cumber [21] reported slow convergence to the numerically exact incident heat flux with oscillations about the numerically exact value as a function of the number of rays.

6. Application of stochastic quadrature schemes

As shown above the ray effect can lead to poor numerical behaviour. If the deterministic quadrature scheme is replaced by a stochastic method such as the reverse Monte Carlo method, then although the ray effect does not arise for the reasons given above the situation is worsened. For convenience in the discussion below the reverse Monte Carlo implementation is labelled $I\cos\sin MC$.

A more efficient quadrature scheme that does not suffer from the ray effect is required.

6.1. Convergence acceleration using Sobol sequences

The $O(N_{\mathrm{Ray}}^{-0.5})$ convergence rate places a severe limitation on the application of the Monte Carlo method. This is recognised by the community of numerical analysts developing Monte Carlo methods and a great deal of effort is directed at improved statistical sampling techniques to accelerate convergence [26,37]. In this spirit it is worthy of note that if the ray directions generated using a pseudo random number generator were space filling but ray avoiding, this would significantly improve the rate of ray convergence. To appreciate why this is the case consider a ray distribution defined by (4),

$$\varphi_i = (i-0.5)\Delta\varphi, \qquad \theta_j = (j-0.5)\Delta\theta \tag{4}$$

where

$$N_{\mathrm{Ray}} = N_\theta \times N_\varphi$$

One way of generating ray directions is to use a pseudo random number generator to choose the ray direction from the prescribed set of rays. Once used a ray orientation is removed from the population before a new ray direction is chosen. Therefore after N_{Ray} rays all rays would have been used. This is essentially an implementation of a deterministic quadrature scheme which has a convergence rate of $O(N_{\mathrm{Ray}}^{-1})$. The order rays are used in a quadrature scheme is irrelevant; however it shows that ray directions that cover the unit hemisphere without ray clustering is beneficial. Sequences of points that cover the integration range more uniformly than uncorrelated pseudo-random number sequences are called quasi-random or sub-random sequences although in reality the self-avoiding property cannot be considered random.

The use of quasi-random numbers that avoid clustering in combination with the Monte Carlo method has been applied in mathematical physics [38] and financial modelling [39] for evaluation of multi-dimensional integrals. The results presented here are an application of a quasi-Monte Carlo method applied to the incident heat flux integral (1). The approach adopted here for generating the ray orientations that are 'ray avoiding' was first suggested by Sobol [40]. The Sobol sequence generation algorithm implemented was developed by Antonov and Saleev [41] and given in [25]. Sobol sequence generation is a mathematically complex process and only a brief overview will be given below. A more detailed description of the process can be found in the references cited. The Sobol sequence generates numbers in the unit interval by an application of exclusive OR (XOR) operations on binary representations of fractions called direction numbers that form a basis. Let the set of direction numbers be denoted,

$$\{V_i\}_{i=1}^{w}$$

where V_i is a binary fraction of length w bits. If S_j denotes the jth number in the Sobol sequence it is calculated by representing j in binary form and applying an XOR operation to all of the direction numbers V_i where i has a nonzero entry in the jth column. This gives the space filling property required as the direction numbers used to generate the Sobol sequence are used with varying frequency of being included and excluded from the set of direction numbers used in the sequence generation. For example, V_1 is used every other Sobol number, V_2 is switched on or off every two Sobol numbers. How the direction numbers are chosen and how the process is implemented in an efficient manner is given in [25].

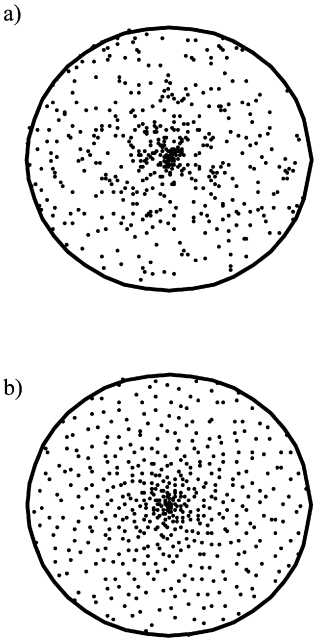

Fig. 4. The first 500 ray orientations calculated using (a) a pseudo random number generator and (b) a Sobol sequence.

Fig. 4a shows the first 500 ray orientations projected onto a disc using a pseudo random number generator to specify ray orientations and using a Sobol sequence to calculate ray orientations. The concentration of rays at the centre of the disc, i.e. the apex of the unit hemisphere is apparent in both ray distributions and is due to the shape of the probability distribution, (3). In Fig. 4a, away from the apex using the pseudo random number generator clusters of points can be identified and corresponding areas on the hemisphere that have not been sampled. In Fig. 4b where ray directions are calculated using a Sobol sequence, away from the apex there is no clustering with a more uniform distribution of rays.

Using Sobol sequences to generate the ray directions can be viewed as an optimal combination of a deterministic quadrature scheme and the reverse Monte Carlo method. Unlike deterministic quadrature schemes a predetermined ray distribution does not

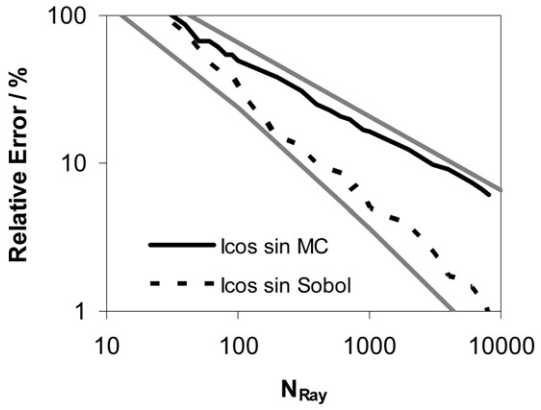

Fig. 5. The relative error for the incident heat flux to the horizontal receiver located at $(r, z) = (0.575\text{ m}, 1\text{ m})$ using $I\cos\sin MC$ and $I\cos\sin Sobol$.

have to be specified in advance. In addition ray convergence does not have to be assessed using a series of finer ray meshes. Comparing the reverse Monte Carlo method using a pseudo random number generator and one using Sobol sequences to calculate the ray directions the convergence rate is significantly accelerated with the latter implementation. Sobol sequences with their space filling property gives an expected convergence rate that asymptotes to $O(N_{\text{Ray}}^{-1})$. It can be proved that if a sub-random sequence is used as part of a Monte Carlo method for evaluating integrals on the hypercube of dimension, d, then the following integral holds,

$$\left| \int_{[0,1)^d} f(\underline{x})\, d\underline{x} - \frac{1}{N}\sum_{i=1}^{N} f(\underline{x}_i) \right| \leqslant \frac{A_1}{N}(\ln N)^d$$

where A_1 is a constant. This is the Koksma–Hlawka inequality [39].

For convenience in the discussion below the implementation of the reverse Monte Carlo method when combined with Sobol sequences is labelled as $I\cos\sin Sobol$. Fig. 5 shows the RMS % error in predicted incident heat flux for the horizontally orientated receiver located at $(r, z) = (0.575, 1)$ as a function of the number of rays using the 'standard' reverse Monte Carlo implementation, $I\cos\sin MC$ and $I\cos\sin Sobol$. As the Monte Carlo method is a stochastic technique for each number of rays, N_{Ray}, 64 samples are used to produce the RMS % error. In addition to the two error curves two further curves of the form,

$$E = AN_{\text{Ray}}^{-0.5}$$

and

$$E = \frac{A}{N_{\text{Ray}}}\ln N_{\text{Ray}}$$

are plotted showing that the expected convergence rates are achieved. The improvement in performance using Sobol sequences for N_{Ray} greater than 100 rays is significant. Further because of the differing convergence rates the more rays used the greater the difference in relative error.

The improved convergence property of the reverse Monte Carlo method combined with Sobol sequences is clear; however the algorithm to generate the ray orientations is more complex than in $I\cos\sin MC$ or the deterministic quadrature scheme. Therefore the computational overhead of the ray orientation calculation must be considered when evaluating the different quadrature schemes. Timing the calculation of the incident heat flux distribution to a vertical line of ten receivers using five hundred rays per receiver for the deterministic quadrature scheme used gave a time of 0.042 seconds per ray. This should be compared with the reverse Monte Carlo method, $I\cos\sin MC$ which required 0.039 seconds per ray and $I\cos\sin Sobol$ which required 0.042 sec per ray. All of the above timing data was taken using a PC with a Dual Intel(R) Core TM 2 processor with a clock speed of 1.8 GHz. It can be seen that the timing data for all three quadrature schemes are similar as the majority of the computation is common to all three schemes. Surprisingly the computational time per ray for the $I\cos\sin MC$ methodology is 7% less than the deterministic quadrature scheme. The reason for this was initially unclear as the operations in the pseudo random number generator are more intensive than the operations to calculate the ray orientations for the deterministic quadrature scheme. A deeper analysis revealed that for $I\cos\sin MC$, the complexity of the ray orientation calculation is compensated for by the fact that the incident flux approximation requires fewer operations than in the deterministic quadrature scheme.

6.2. Sobol sequences and confidence limits

The accelerated convergence using Sobol sequences is welcome but it has come at a price as the Central Limit Theorem cannot be used to calculate a confidence interval. It is not possible to prove a strong result akin to the Central Limit Theorem although it seems reasonable to expect the variable,

$$z_j = \frac{AN_{\text{Ray}}}{\ln(N_{\text{Ray}})}\frac{(\overline{I^-_{N_{\text{Ray}}}} - \overline{I^-_{N_{\text{Ray}},j}})}{\sigma_{I\cos\sin}} \tag{5}$$

$$\overline{I^-_{N_{\text{Ray}},j}} = \frac{1}{N_{\text{Ray}}}\sum_{i=1}^{N_{\text{Ray}}} I^-(\varphi_i, \theta_i)\cos\theta_i \sin\theta_i \tag{6}$$

$$\overline{I^-_{N_{\text{Ray}}}} = \frac{1}{N_{\text{Sample}}}\sum_{j=1}^{N_{\text{Sample}}} \overline{I^-_{N_{\text{Ray}},j}}$$

for some value of A to have a Gaussian or near Gaussian distribution. This is a heuristic rule rather than a theorem that has been found to have some generality. It has been verified to be true for a range of receiver locations and orientations, different numbers of rays up to 1000 and different sample sizes up to 10,000 in combination with the Monte Carlo implementation, $I\cos\sin Sobol$, for

$$A = 0.75$$

Fig. 6 shows the calculated probability distribution for z_j, (5) combined with $I\cos\sin Sobol$ with a Gaussian distribution for the receiver $(r, z) = (0.575, 1)$. The calculated distribution is from a sample of 1000, with $N_{\text{Ray}} = 300$. For comparison the calculated distribution for the equivalent of z_j, for $I\cos\sin MC$ is also shown. The $I\cos\sin MC$ distribution can be thought of as a 'control' as the Central Limit Theorem holds. Overall the level of agreement with the Gaussian distribution for both Monte Carlo implementations is similar.

As far as deriving rigorous confidence intervals the important property is not so much the Gaussian distribution more the area under the Gaussian curves, for given integration bounds. Fig. 7 shows a comparison of the area under the Gaussian curve compared to a quadrature of the calculated probability density functions shown in Fig. 6. The numerical integration shows a partial cancelation of over and under prediction of the Gaussian distribution to produce good agreement between the analytic curve and $I\cos\sin MC$, and $I\cos\sin Sobol$.

This is an important result as it means a confidence interval for a predicted incidence heat flux prediction using Sobol sequences can be calculated. For example, for a 95% confidence limit the predicted incident heat flux is expected to satisfy the following inequality for 95% of the heat fluxes evaluated using $I\cos\sin Sobol$,

$$\left|q_{\text{inc,act}} - q_{\text{inc,pred}}(N_{\text{Ray}})\right| \leqslant \frac{1.96\pi^2\sigma_{I\cos\sin}\ln(N_{\text{Ray}})}{AN_{\text{Ray}}}$$

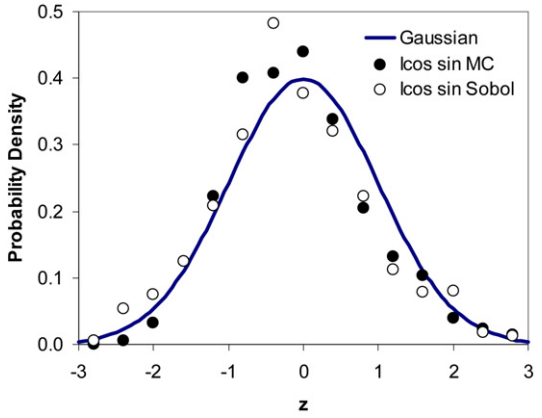

Fig. 6. Probability distribution for the Gaussian variable calculated using $I\cos\sin MC$ and $I\cos\sin Sobol$, sample $= 1000$, $N_{\text{Ray}} = 300$.

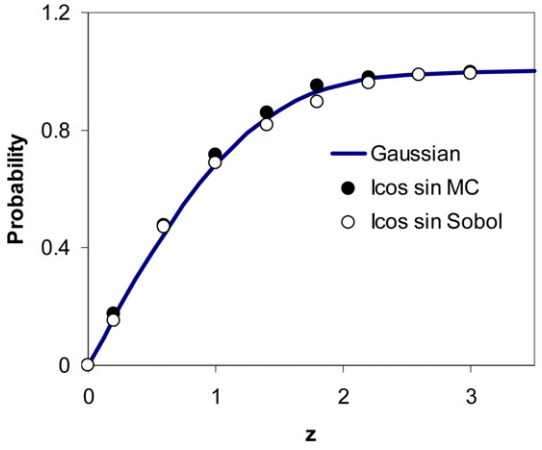

Fig. 7. Integrated probability distribution calculated using $I\cos\sin MC$ and $I\cos\sin Sobol$, sample $= 1000$, $N_{\text{Ray}} = 300$.

Fig. 8 shows the predicted heat flux with a 95% confidence interval for the receiver located at $(r, z) = (0.575, 1)$ for both $I\cos\sin MC$ and $I\cos\sin Sobol$. For the simulations using Sobol sequences the rapidly diminishing size of the confidence interval as the number of rays increases is apparent. For 8000 rays the 95% confidence interval is 3% of the predicted incident heat flux using $I\cos\sin Sobol$ compared to 23% for 8000 rays using $I\cos\sin MC$. Alternatively using $I\cos\sin Sobol$ it requires 800 rays to achieve a 95% confidence interval of 23% of the predicted incident heat flux.

7. An adaptive stochastic quadrature scheme

It is possible to combine $I\cos\sin Sobol$ with ray adaptivity exploiting the shape of the intensity distribution to a receiver. The intensity distribution to a receiver located in the far field and relatively close to a jet fire is significant over a small part of the receiver field of view. The remaining intensity distribution is made up of the background intensity,

$$I_{bg} = \sigma \frac{T_{\text{amb}}^4}{\pi}$$

Recognising this fact the incident flux integral can be modified to

$$q_{\text{inc}} = \int_{I^- > I_{bg}} I^- \cos\theta \, d\Omega + I_{bg} \int_{I^- = I_{bg}} \cos\theta \, d\Omega$$

where $d\Omega$ represents a differential solid angle on the unit hemisphere. One way forward is to separate the range of integration into two sets, a hot ray set, $S_{\text{hot ray}}$ and a cold ray set, $S_{\text{cold ray}}$,

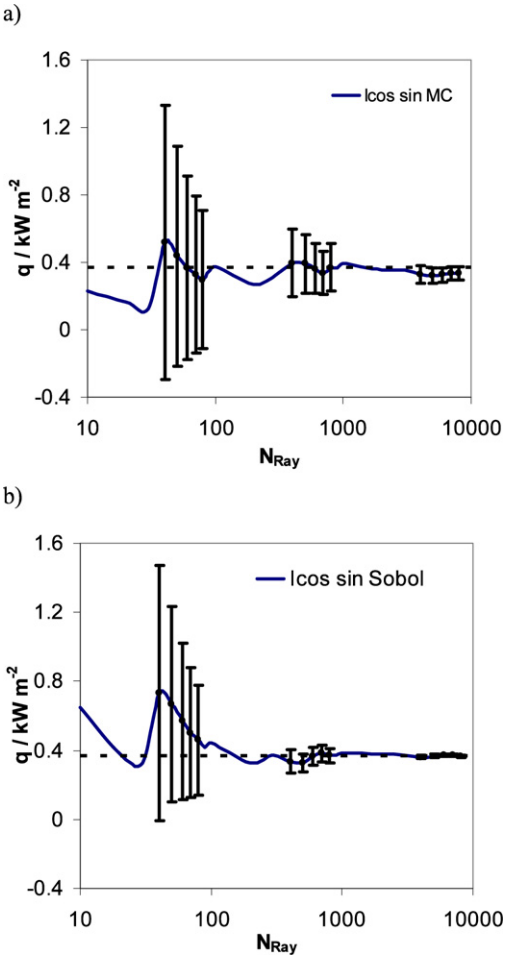

Fig. 8. Predicted incident heat flux for an horizontally orientated receiver located at $(r, z) = (0.575\text{ m}, 1\text{ m})$ with a 95% confidence limit vs. number of rays, a) calculated using $I\cos\sin MC$ and (b) calculated using $I\cos\sin Sobol$.

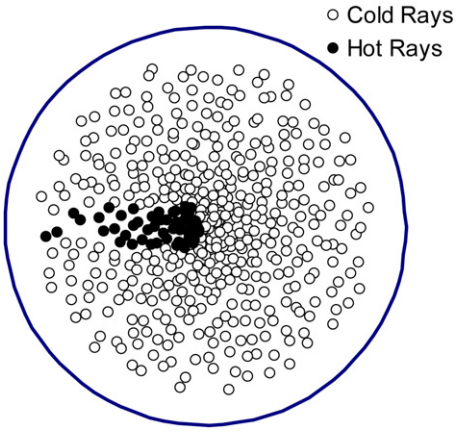

Fig. 9. The first 500 ray orientations separated into the hot and cold ray sets for the vertical receiver located at (0.55 m, 0. m).

$$S_{\text{hot ray}} = \left\{(\varphi, \theta), I^-(\varphi, \theta) > I_{bg}\right\}$$

$$S_{\text{cold ray}} = \left\{(\varphi, \theta), I^-(\varphi, \theta) = I_{bg}\right\}$$

Fig. 9 shows the hot and cold ray sets for the first 500 rays from a vertical receiver located at $(r, z) = (0.55, 0)$.

The key idea behind the adaptive stochastic algorithm presented below is rays traced previously are divided into hot rays and cold rays. Given a new ray orientation (φ_R, θ_R), determine if

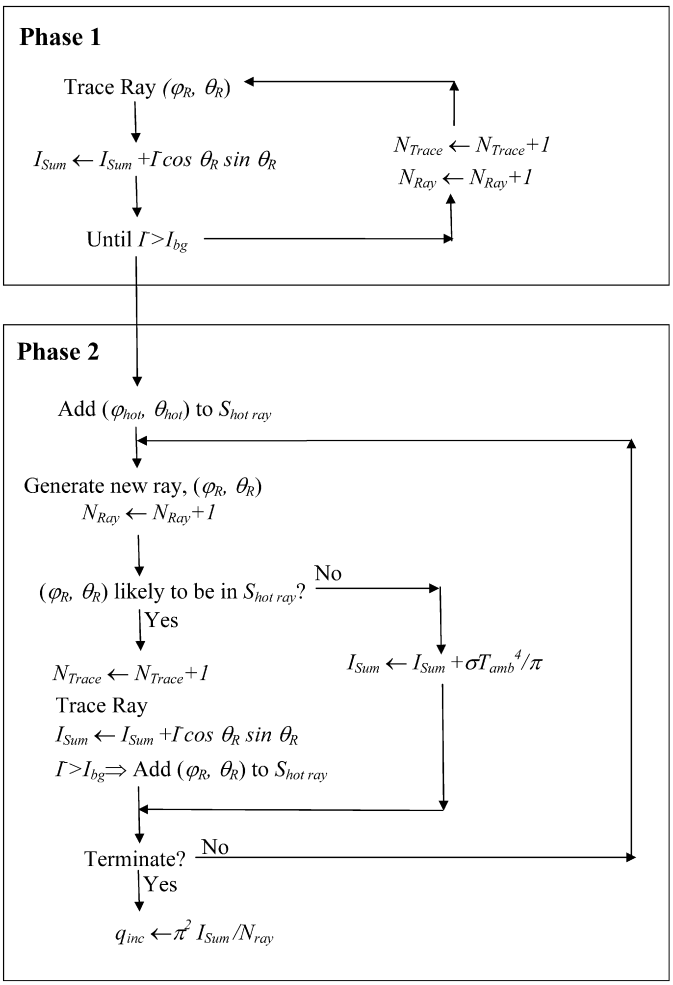

Fig. 10. The adaptive stochastic algorithm, *I* cos sin *Adaptive*.

the new ray is likely to be in the hot ray set. If the new ray is likely to be in the hot ray set then it is traced, the equation of radiative heat transfer solved and the spectral intensity distribution integrated otherwise the term,

$$\sigma \frac{T_{\text{amb}}^4}{\pi} \cos\theta_R \sin\theta_R$$

is added to the summation (6) making a significant computational saving.

7.1. Adaptive stochastic algorithm

An outline of the adaptive stochastic algorithm is given in Fig. 10 and a description of the more important details of implementation given below. The algorithm given in Fig. 10 is executed in two phases. The first phase is conventional *I* cos sin *Sobol*. The second phase occurs once the hot ray set exists, i.e. a ray is traced with an incident intensity value above the background intensity. In the second phase the hot ray set grows and only a proportion of rays generated are traced. Ideally during the second phase only hot rays are traced, in reality as the hot ray set is characterised in more detail the proportion of hot rays traced compared to the total number of rays traced increases.

Two points of implementation require further discussion. The set of hot rays are stored as,

$$S_{\text{hot ray}} = \{(X_j, Y_j),\ \ j = 1, 2, \ldots, N_{\text{hot}}\}$$

using the transformed variables

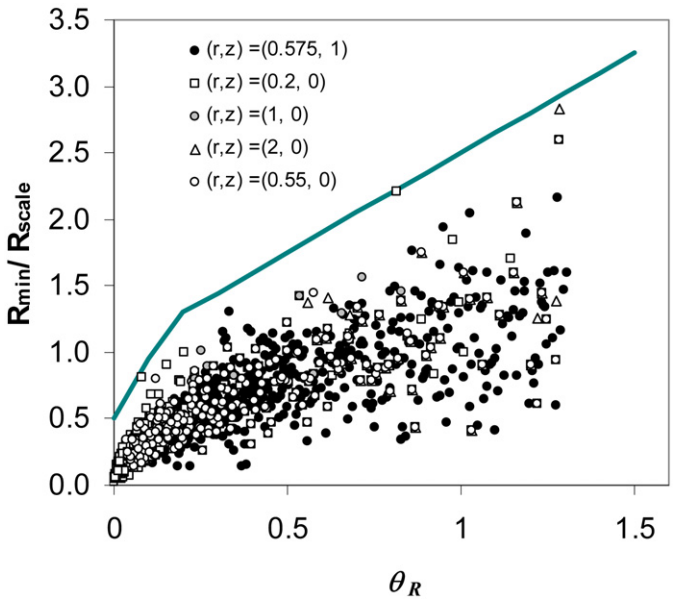

Fig. 11. Minimum distances to the hot ray set for a number of rays and receiver locations.

$$X_j = \theta_j \cos\varphi_j$$
$$Y_j = \theta_j \sin\varphi_j \tag{7}$$

This is done as it is easier to derive a methodology for determining if a new ray, (φ_R, θ_R) is likely to be in the hot ray set, $S_{\text{hot ray}}$. Working with the transformed variables (X_R, Y_R) the ray is considered likely to be in the hot ray set if,

$$\sqrt{(X_R - X_j)^2 + (Y_R - Y_j)^2} < f(N_{\text{Ray}}, \theta_R) \quad \text{for some } j \in S_{\text{hot ray}}$$

where the function f is yet to be specified. The dependence on θ_R is required as the distribution of rays on the unit hemisphere is biased towards the apex and the transformation (7) is not conservative. Similarly as the number of rays, N_{Ray} increases we would expect the hot ray set to more accurately characterise the intensity distribution where the incident intensity is significant. Therefore on the grounds of efficiency we require a function that has the property that as the number of rays, N_{Ray} increases f decreases.

To make progress we make f a separable function,

$$f(N_{\text{Ray}}, \theta_R) = g(N_{\text{Ray}})h(\theta_R)$$

The functional form for g is determined by deriving a length scale, R_{scale},

$$g(N_{\text{Ray}}) = R_{\text{scale}} = \sqrt{\frac{2\pi}{N_{\text{Ray}}}}$$

To determine a candidate function for $h(\theta_R)$, for a range of receiver locations the minimum distance to the hot ray set was calculated.

$$R_{\min} = \min\left\{\sqrt{(X_R - X_j)^2 + (Y_R - Y_j)^2},\ \ j \in S_{\text{hot ray}}\right\}$$

The results are plotted in Fig. 11. A function that is relatively simple to implement and is an upper bound for $R_{\min}(\theta_R)$ is

$$h(\theta_R) = \min\{4.5\theta_R + 0.5, 1.5\theta_R + 1\}$$

All of the elements of the algorithm are now in place. The adaptive quadrature algorithm for convenience is labelled as *I* cos sin *Adaptive* in the discussion below.

Fig. 12 shows the relative error as a function of rays traced, for a vertical receiver located at (0.55, 0). For comparison *I* cos sin *MC* and *I* cos sin *Sobol* are shown together with *I* cos sin *Adaptive*. The

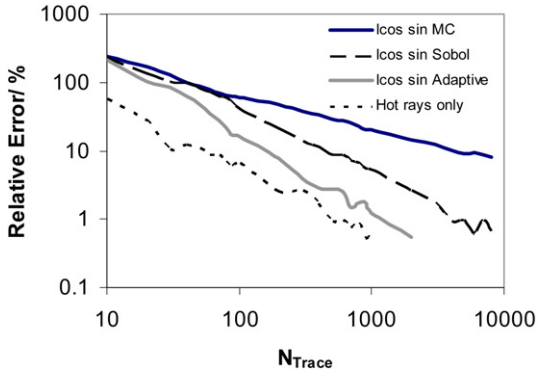

Fig. 12. The relative error for the incident heat flux to the vertical receiver located at $(r, z) = (0.55\ \text{m}, 0\ \text{m})$ using $I\cos\sin$ *MC*, $I\cos\sin$ *Sobol*, $I\cos\sin$ *Adaptive* and hot rays only.

fourth line shown, is labelled 'hot rays only', in this case the RMS error is plotted against the number of hot rays traced. Of course for the hot ray case there is no way a priori of determining if a ray is a hot or cold ray before it is traced. The hot ray error curve provides an indication of how efficient $I\cos\sin$ *Adaptive* is, as it represents the best solution possible where every ray traced is a hot ray.

From Fig. 12 it is clear that for a small number of rays traced, $I\cos\sin$ *Adaptive* gives results similar to $I\cos\sin$ *Sobol*. For a larger number of rays traced $I\cos\sin$ *Adaptive* is a significant improvement over $I\cos\sin$ *Sobol*. As the number of rays traced increases the $I\cos\sin$ *Adaptive* error curve is closer to the hot ray curve than to the $I\cos\sin$ *Sobol* error curve. This is consistent with the improved characterisation of the intensity distribution by the hot ray set as the number of rays increases.

To quantify the improvement in ray convergence rate, for the standard Monte Carlo method, $I\cos\sin$ *MC*, a relative RMS error of approximately 8% is achieved with 8000 rays for the vertical receiver located at $(r, z) = (0.55\ \text{m}, 0\ \text{m})$. To achieve the same relative RMS error $I\cos\sin$ *Sobol* requires 700 rays. The new adaptive methodology, $I\cos\sin$ *Adaptive* requires 200 rays to achieve the same relative RMS error. This potentially represents a speed-up of 40 times for $I\cos\sin$ *Adaptive* compared to the standard Monte Carlo method, $I\cos\sin$ *MC*; however it should be appreciated that for each ray there is a small overhead associated with the calculation of the likelihood that a ray is a member of the hot ray set.

8. Conclusion

In this paper the calculation of the incident heat flux to a target external to the fire is considered using a modification of the reverse Monte Carlo method. The modified reverse Monte Carlo method addresses the main weakness of the Monte Carlo method, its slow convergence rate, $O(N_{\text{Ray}}^{-0.5})$. This was done by replacing the pseudo random number generator for calculating ray orientations with a ray direction specification based on Sobol sequences. Sobol sequences produce points on the unit hemisphere that are not independent of each other in that new points in the sequence avoid points generated previously. This has the property that a more uniform pattern of rays on the unit hemisphere is produced, giving a ray convergence rate for the incident heat flux of $O(N_{\text{Ray}}^{-1}\ln(N_{\text{Ray}}))$.

The use of Sobol sequences to generate ray directions means that the Central Limit Theorem no longer holds. In its place it is possible to construct a Gaussian variable from the incident intensity distributions calculated using Sobol sequences. This makes it possible to calculate confidence limits for a prediction of incident heat flux and the confidence limits contract with ray number at a rate of $O(N_{\text{Ray}}^{-1}\ln(N_{\text{Ray}}))$.

A new algorithm for evaluating the incident heat flux more efficiently has also been proposed that builds on the use of Sobol sequences by exploiting the shape of the incident intensity distribution to receivers surrounding jet fires. The new algorithm, $I\cos\sin$ *Adaptive* is more efficient than the standard implementation of the Monte Carlo method implemented with Sobol sequences as a large proportion of the rays generated are not traced making a significant saving. In addition the further the receiver is from the fire the smaller the field of view that the intensity is above back ground radiation levels improving the efficiency of $I\cos\sin$ *Adaptive* as fewer rays are traced as a proportion of the total number of rays generated.

References

[1] D. Drysdale, Introduction to Fire Dynamics, 2nd ed., Wiley, UK, 1998.
[2] D.K. Cook, P.S. Cumber, M. Fairweather, F. Shemirani, Modelling free and impacting underexpanded jet fires, in: IChemE Symposium Series, vol. 141, The Institution of Chemical Engineers, Rugby, 1997, pp. 127–138.
[3] S.M. Jeng, L.D. Chen, G.M. Faeth, The structure of buoyant methane and propane diffusion flames, in: Nineteenth Symposium (International) on Combustion, The Combustion Institute, Pittsburgh, 1982, pp. 349–358.
[4] S.M. Jeng, M.C. Lai, G.M. Faeth, Nonluminous radiation in turbulent buoyant axisymmetric flames, Combust. Sci. and Tech. 40 (1984) 41–53.
[5] G.T. Kalghatgi, Lift-off heights and visible lengths of vertical turbulent jet diffusion flames in still air, Combust. Sci. and Tech. 41 (1984) 17–29.
[6] P.S. Cumber, M. Spearpoint, Modelling lifted methane jet fires using the boundary layer equations, Journal of Numerical Heat Transfer, Part B 49 (2006) 239–258.
[7] O. Onokpe, P.S. Cumber, Modelling lifted hydrogen jet fires using the boundary layer equations, in: Proceedings of the 10th UK Heat Transfer Conference, Edinburgh 2007.
[8] R.P. Cleaver, P.S. Cumber, M. Fairweather, Predictions of sonic jet fires, Combust. Flame 132 (2003) 463–474.
[9] F.C. Lockwood, N.G. Shah, A new radiation solution method for incorporation in general combustion prediction procedures, in: Eighteenth Symposium (International) on Combustion, The Combustion Institute, Pittsburgh, 1981, pp. 1405–1414.
[10] P.S. Cumber, Improvements to the discrete transfer method of calculating radiative heat transfer, International Journal of Heat and Mass Transfer 38 (1995) 2251–2258.
[11] M.F. Modest, Backward Monte Carlo simulations in radiative heat transfer, ASME J Heat Transfer 125 (2003) 57–62.
[12] M.Y. Choi, A. Hamins, H. Rushmeier, T. Kashiwagi, Simultaneous optical measurement of soot volume fraction, temperature and CO_2 in heptane pool fire, in: Twenty Fifth Symposium (International) on Combustion, The Combustion Institute, Pittsburgh, 1994, pp. 1471–1480.
[13] G. Cox, On radiant heat transfer from turbulent flames, Combust. Sci. Tech. 17 (1977) 75–78.
[14] P.S. Cumber, M. Fairweather, S. Ledin, Application of wide band radiation models to non-homogeneous combustion systems, International Journal of Heat and Mass Transfer 41 (1998) 1573–1584.
[15] R. Siegel, J.R. Howell, Thermal Radiation Heat Transfer, 3rd ed., Hemisphere Publishing Corporation, 1992.
[16] J.C. Chai, S.L. Haeok, S.V. Patankar, Ray effect and false scattering in the discrete ordinates method, Numerical Heat Transfer, Part B 24 (1993) 373–389.
[17] K.D. Lathrop, Ray effects in discrete ordinates equations, Nuclear Science and Engineering 32 (1968) 357–369.
[18] K.D. Lathrop, Remedies for ray effects, Nuclear Science and Engineering 45 (1971) 255–268.
[19] W.A. Fiveland, Three-dimensional radiative heat transfer solutions by the discrete-ordinates method, J. of Thermophysics 2 (1988) 309–316.
[20] S.M. Jeng, G.M. Faeth, Radiative heat fluxes near turbulent buoyant methane diffusion flames, ASME J. Heat Transfer 106 (1984) 886–888.
[21] P.S. Cumber, Ray effect mitigation in jet fire radiation modelling, International Journal of Heat and Mass Transfer 43 (2000) 935–943.
[22] P.S. Cumber, Application of adaptive quadrature to fire radiation modelling, ASME J. Heat Transfer 121 (1999) 203–205.
[23] H.K. Versteeg, J.C. Henson, W. Malalasekera, An adaptive angular quadrature for the discrete transfer method based on error estimation, ASME J. Heat Transfer 125 (2003) 2301–2311.
[24] L. Ben-wen, T. Wen-quan, Ray effect in ray tracing method for radiative heat transfer, International Journal of Heat and Mass Transfer 40 (1997) 3419–3426.
[25] W.H. Press, S.A. Teukolsky, W.T. Vetterling, B.P. Flannery, Numerical Recipes in Fortran 77, 2nd ed., Cambridge University Press, 1992.

[26] T. Pang, An Introduction to Computational Physics, Cambridge University Press, 1997.
[27] W.L. Grosshandler, Radiative heat transfer in non-homogeneous gases: A simplified approach, International Journal of Heat and Mass Transfer 23 (1980) 1447–1459.
[28] W.L. Grosshandler, RADCAL: A narrow-band model for radiation calculations in a combustion environment, NIST Technical Note 1402, 1993.
[29] P.S. Cumber, M. Fairweather, Evaluation of flame emission models combined with the discrete transfer method for combustion system simulation, International Journal of Heat and Mass Transfer 48 (2005) 5221–5239.
[30] D.B. Spalding, GENMIX: A General Computer Program for Two-Dimensional Parabolic Phenomena, Pergamon Press, Oxford, 1977.
[31] M. Fairweather, W.P. Jones, S. Ledin, P. Lindstedt, Predictions of soot formation in turbulent non-premixed propane flames, in: Twenty Fourth Symposium (International) on Combustion, The Combustion Institute, Pittsburgh, 1992, pp. 1067–1074.
[32] W.P. Jones, B.E. Launder, The prediction of laminarization with a two equation model of turbulence, International Journal of Heat and Mass Transfer 15 (1972) 301–314.
[33] S.B. Pope, An explanation of the turbulent round-jet/plane-jet anomaly, AIAA J. 16 (1978) 279–281.
[34] J.B. Moss, C.D. Stewart, K. Syed, Flow field modelling of soot formation at elevated pressure, in: Twenty Second Symposium (International) on Combustion, The Combustion Institute, Pittsburgh, 1988, pp. 413–423.
[35] M. Fairweather, W.P. Jones, R.P. Lindstedt, Predictions of radiative heat transfer from a turbulent reacting jet in a cross-wind, Combust. Flame 89 (1992) 45–63.
[36] P.S. Cumber, M. Spearpoint, A computational flame length methodology for propane jet fires, Fire Safety Journal 41 (2007) 215–228.
[37] E. Lapeyre, E. Pardoux, R. Sentis, Introduction to Monte Carlo methods for transport and diffusion equations, 1998.
[38] B.D. Keister, Multidimensional quadrature algorithms, Computers in Physics 10 (1996) 119–122.
[39] P. L'Ecuyer, Quasi-Monte Carlo methods in finance, in: R.G. Ingalls, M.D. Rossetti, J.S. Smith, B.A. Peters (Eds.), IEEE, Proceedings Winter Simulation Conference, 2004, pp. 1645–1655.
[40] I.M. Sobol, Uniformly distributed sequences with an additional uniform property, USSR Computational Mathematics and Mathematical Physics 16 (1977) 236–242.
[41] I.A. Antonov, V.M. Saleev, An economic method of computing LP tau-sequences, USSR Computational Mathematics and Mathematical Physics 19 (1979) 252–256.